Microscopic Investigation of RF Surfaces of 3 GHz Niobium Accelerator Cavities Following RF Processing*

J. Graber‡, P. Barnes, T. Flynn, J. Kirchgessner, J. Knobloch, D. Moffat, H. Muller, H. Padamsee, and J. Sears
F.R. Newman Laboratory of Nuclear Studies
Cornell University
Ithaca, NY 14853 USA

Abstract

RF processing of Superconducting accelerating cavities is achieved through a change in the electron field emission (FE) characteristics of the RF surface. We have examined the RF surfaces of several single-cell 3 GHz cavities, following RF processing, in a Scanning Electron Microscope (SEM). The RF processing sessions included both High Peak Power ($P \leq 50$ kW) pulsed processing, and low power (≤ 20 W) continuous wave processing. The experimental apparatus also included a thermometer array on the cavity outer wall, allowing temperature maps to characterize the emission before and after RF processing gains. Multiple sites have been located in cavities which showed improvements in cavity behavior due to RF processing. Several SEM-located sites can be correlated with changes in thermometer signals, indicating a direct relationship between the surface site and emission reduction due to RF processing. Information gained from the SEM investigations and thermometry are used to enhance the theoretical model of RF processing.

I. INTRODUCTION

The HPP experimental program was initiated in order to investigate high power RF processing as a method of reducing and understanding field emission in superconducting accelerator cavities. Results of this program have been presented at previous and present Particle Accelerator Conferences.[1],[2] An extensive description of the entire HPP program can be found in the recently completed Ph.D. dissertation associated with this work.[3]

We report here on the effort to characterize the microscopic effects of RF processing. Surface investigation studies of the cavities in the HPP program was initiated with the goal of finding physical evidence of processing on the RF surface. We were encouraged by the findings of the Mushroom cavity project[4] at Cornell, in which a specially designed, nonaccelerating cavity was examined in a Scanning Electron Microscope (SEM) following RF cold tests. Multiple phenomena were encountered in the high electric field regions of the cavity, indicating a strong link to field emission activity.

In order to better establish the link between surface features and RF processing, the experimental apparatus included an array of 100 thermometers placed in ten boards of ten resistors, spaced at 36 degree intervals around the azimuth of the cavity. Thermometers such as these have been a common diagnostic tool in SRF work for the last ten years.

SEM investigation of the cavities involves dissection of the single cell cavities in order to facilitate investigation of the RF surface, and is the final step performed on a test cavity.

II. PHYSICAL EVIDENCE OF RF PROCESSING

Ultimately it is desirable to gather microscopic information on field emission sites. DC field emission studies[5] have shown that these are micron or submicron features, for example, superficial particles. Even with guidance from thermometry, where the resolution is of the order of a few square millimeters, location of such minuscule features after dissection of a cavity presents a significant challenge. Fortunately, as this study shows, if the emission site processes, or undergoes significant change during cavity operation, then the additional features associated with the processing event make it substantially easier to locate the site.

Several sites were found which have both a significant thermometry signal, a change in signal after processing, and an associated surface feature. One example stands out above the rest, as the clearest processing event, therefore we will expand upon this site here. This site was found in a cavity (designated 1-5) which was RF tested specifically with the goal of limiting the run to one or two processing events. More examples of SEM located processing sites, as well as other phenomena can be found in references [3] and [6].

Figure 1 shows the Q_0 vs. E_{peak} plots from the three CW power rises of this experiment. The initial CW power rise was limited by heavy FE at $E_{peak} = 32$ MV/m. HPP processing was then performed with $P_{RF} = 2$ kW, $t_{RF} = 630$ µsec. Peak fields during processing reached 49 MV/m. The second CW measurement was limited at 34 MV/m, again by heavy FE. The second HPP session was performed with $P_{RF} = 3.5$ kW, $t_{RF} = 630$ µsec. Peak fields during processing reached 54 MV/m. In the final CW session, E_{peak} reached 36 MV/m, again limited by FE.

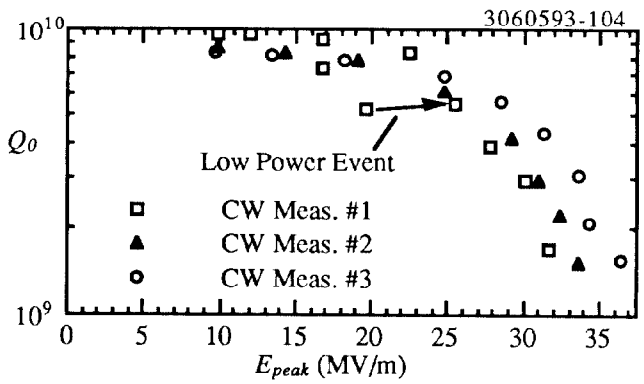

Figure 1. Q_0 vs. E_{peak} curves from low power measurements on single-cell cavity 1-5.

* Supported by the NSF with supplementary support from the U.S.-Japan Collaboration.

‡ Permanent Address: DESY, 85 Notkestrasse, 2000 Hamburg 52, Germany.

0-7803-1203-1/93$03.00 © 1993 IEEE

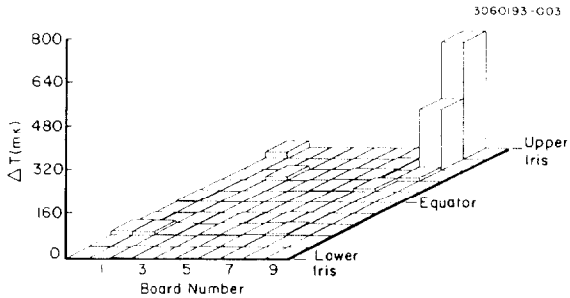

Figure 2. Temperature map measured at E_{peak} = 31 MV/m in the first CW power rise.

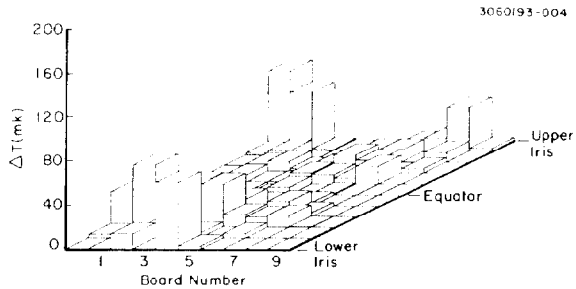

Figure 3. Temperature map measured at E_{peak} = 36 MV/m in the final CW power rise, following HPP processing.

Figure 2 is a temperature map of the cavity taken during the first CW measurements, at E_{peak} = 32 MV/m. The temperature map shows that the cavity was clearly dominated by a single emission site, located near the upper iris of the cavity board number 8. Figure 1 shows that, in addition to HPP processing, a processing event took place in the initial CW rise of the cavity, marked by the arrow. Inspection of the temperature maps reveal that this event was accompanied by a reduction in the heating at the dominant site shown in Figure 2.

Figure 3 is a temperature map taken during the final CW measurement, at E_{peak} = 36 MV/m. Note the reduced scale of the plot. While emission is still present, the site at the upper iris of board 8 is no longer dominating the cavity behavior. The change in heating is attributed to a change in FE characteristics through RF processing.

Given the measured change in heating, we then model the emission heating characteristics, before and after RF processing. In order to model the emission heating, we use a simulation[7] which assumes that the emission current is consistent with the enhanced Fowler-Nordheim (F-N) theory of emission:

$$I_{FN} = \frac{C A}{\phi} (\beta E)^2 \exp\left(-\frac{B \phi^{\frac{3}{2}}}{\beta E}\right) \quad (1)$$

where I_{FN} is the FE current, E is the local surface electric field, ϕ is the work function of the metal, C and B are constants and β and A are the F-N field enhancement factor and emitter area, respectively. The present best model of the enhancement allows for both geometrical and material mechanisms of field enhancement. Furthermore, while no definite physical significance can be attributed to β or A, they are still useful quantities for characterizing the nature of emitters.

We therefore wish to extract values of β and A in order to better understand RF processing and its effect on emission

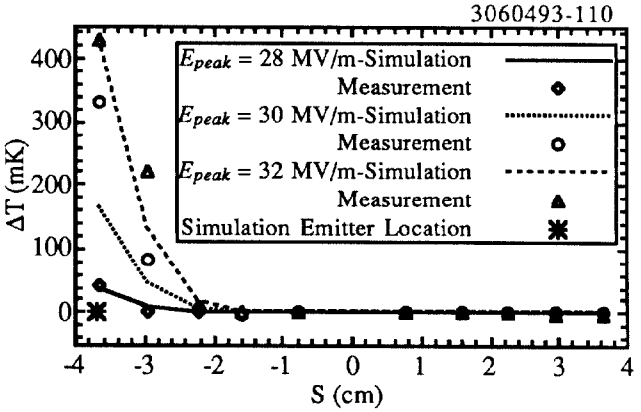

Figure 4. Comparison of measured and simulated temperature along board 8, in the first CW power rise.

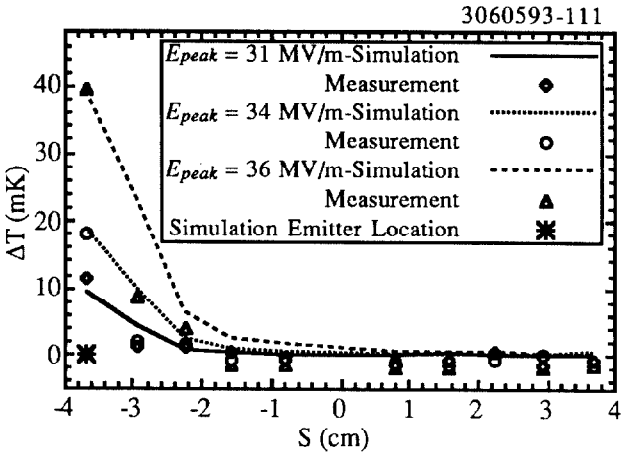

Figure 5. Comparison of measured and simulated temperature along board 8, in the final CW power rise.

sites. The method of extracting these values is to vary β and A in the simulation to best match the simulated with measured temperature signals on the cavity over several different electric field values. The field distribution of the fundamental mode of a cavity is such that emitted electrons follow trajectories with no azimuthal change, therefore all heating due to an emission site will be along a single board. S is the distance from the cavity equator along the cavity surface.

Figures 4 and 5 show the measured and simulated temperature signals along board 8 for the initial and final CW measurements on cavity 1-5, respectively. Simulation of the initial CW rise assumes the emission source at S = -3.7, β = 200, and $A = 3.2 \times 10^{-9}$ cm^2. The simulation of the final CW power rise assumes S = -3.7, β = 300, and $A = 1 \times 10^{-13}$ cm^2.

Given this agreement between measured and simulated thermometry, the cavity was dissected and put into the SEM, for examination in the region indicated as the processed emission site. The examination was successful, as one "starburst" feature was detected. Photographs of this starburst are shown in Figures 6 and 7. No other surface phenomena were detected in a position to eplain the change in emission characteristics.

As with most starbursts, the feature is dominated by a darkened (as viewed in the SEM) burst region, with diameter approxiamtely 200 microns. At the center of this starburst are

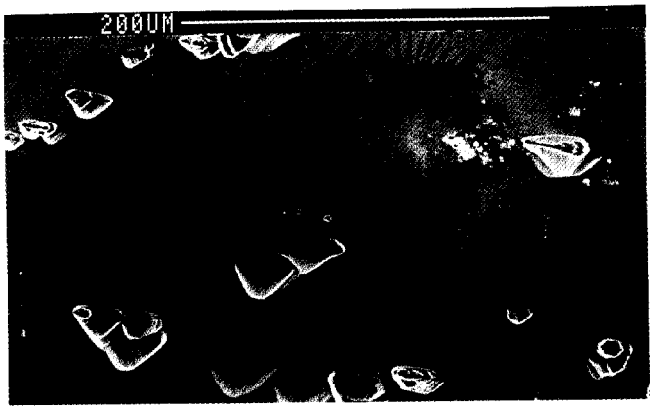

Figure 6. SEM photograph of the starburst region found in cavity S3C1-5. The starburst and craters are located in a position to explain the processing event.

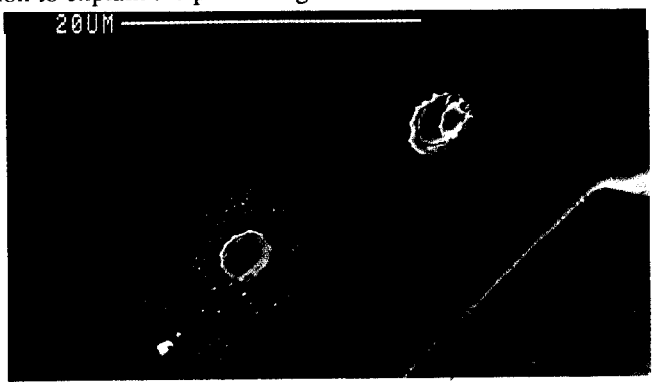

Figure 7. SEM photograph of the central region of Figure 6. Contaminant materials include Ca, Ti, C, and O.

several small (10 microns) crater regions, which appear to have become molten. The craters are shown in Figure 7.

The working model for RF processing, and the creation of a starburst is that as fields are increased, the emission current increases until the resistive losses become so high that the emitter melts/vaporizes. The event appears to be explosive in nature, as evidenced by the splash appearance of many crater regions. A more complete description of this model can be found in references [3] and [6].

Examination of X-ray information in the SEM indicate that contaminant materials at this site include Calcium, Carbon, Oxygen, and Titanium. The crystalline appearing features are called "etch pits," and are an pitting phenomena which occur frequently in cavities which are acid etched following high temperature baking. These pits appear throughout the cavity, and therefore are not thought to be significant to cavity behavior.

In all, we have examined 6 cavities following HPP processing. The general rule we have found is that the higher the fields that the cavity is exposed to, the more starbursts are found. This is consistent with the model presented above, as higher fields are capable of processing more sites.

This phenomena is demonstrated more conclusively, by examining the radial distribution of starbursts in the cavities. Figure 8 shows such a distribution, superimposed with the relative electric field as a function of radius and aligned with a

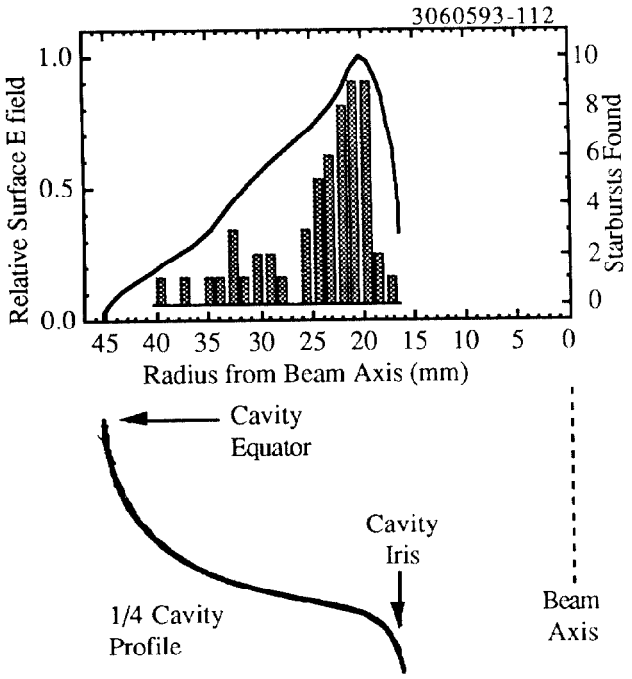

Figure 8. Radial distribution of "Starburst" phenomena found in all examined single-cell cavities, plotted along with relative surface electric field.

TABLE 1: CONTAMINANT ELEMENTS FOUND IN STARBURSTS IN HPP CAVITIES

Element	Starbursts	Element	Starbursts
Indium	19	Calcium	1
Iron	11	Silicon	1
Copper	4	Oxygen	1
Chromium	2	Carbon	1
Titanium	2		

quarter cavity profile. The starbursts are well concentrated in the high field region of the cavity, again supporting the model presented above.

Finally, in Table 1, we present a listing of the various contaminant materials detected in starburst in single-cell cavities.

III. ACKNOWLEDGMENTS

The authors thank Karen Sauer, Will Dickinson, and Adam Leibovich for their assistance on the thermometry portions of the HPP set-up.

IV. REFERENCES

1 J. Graber, et al., *Proc. of the 1991 Particle Accelerator Conference*, IEEE Cat. No. **91CH3038-7**, 2411 (1991).
2 J. Graber, et al., this conference, posters Sa42 and Sa44.
3 J. Graber, Ph.D. Dissertation, Cornell University (1993).
4 D. Moffat, Cornell Report **CLNS 90/991** (1990).
5 Ph. Niedermann, Ph.D. Thesis No. 2197, U. of Geneva (1986).
6 D. Moffat, et al., *Proc. of the 5th Workshop on RF Superconductivity*, D.Proch ed., DESY, Hamburg, Germany, **DESY M-92-01**, 245 (1992).
7 Cornell Report **CLNS/D 910121/24**, W. Hartung ed. (1989).